Optimization of Spot Weld Joining Parameters for Dissimilar Plate Materials through Finite Element Model Updating and Response Surface Methodology

*R.M. Yaacob, J.M. Zikri, N.A.Z. Abdullah, M.S.M. Sani**
Faculty of Mechanical and Automotive Engineering Technology,
Universiti Malaysia Pahang Al-Sultan Abdullah,26600 Pekan, Pahang, MALAYSIA
**mshahrir@umpsa.edu.my*

Muhamad Norhisham Abdul Rani
School of Mechanical Engineering, College of Engineering,
Universiti Teknologi MARA (UiTM), Shah Alam, 40450, MALAYSIA

Ellyawan Setyo Arbintarso
Fakultas Teknik Mesin, Institut Sains & Teknologi Akprind, Jl. Kalisahak 28
Yogyakarta, INDONESIA

ABSTRACT

The utilization of dissimilar materials in manufacturing processes, especially in the automotive and aerospace industries, offers substantial benefits such as weight reduction, improved fuel efficiency, and enhanced mechanical properties. However, the optimization of spot welds for these dissimilar materials presents significant challenges due to their diverse physical and chemical properties. This research seeks to optimize the input properties of finite element models (FEM) for spot welding dissimilar plates by utilizing model updating and response surface methodology (RSM). These techniques refine the computational models to more accurately reflect experimental data. Correlation techniques were used to compare Experimental Modal Analysis (EMA) and Finite Element Analysis (FEA), revealing that CWELD has a 1.21% higher correlation compared to CBAR and CBEAM. Despite this, CWELD was chosen for the updating process due to its similarity with the actual joining structure. Subsequent Finite Element Model Updating

ISSN 1823-5514, eISSN 2550-164X

https://doi.org/10.24191/jmeche.v13i1.2970

Received for review: 2024-06-30
Accepted for publication: 2024-09-13
Published: 2024-11-15

(FEMU) effectively reduced the error in natural frequency prediction from 6.87% to 4.04%. Additionally, the RSM approach successfully optimized the structural design variables, achieving a desirability rate of 0.972 and showing a significant reduction in percentage error to 5.02% from 6.87%. This study offers valuable insights into the effective enhancement of dynamic properties for dissimilar plate structures, highlighting the importance of both optimization techniques in achieving superior accuracy in structural analysis and design.

Keywords: *Dissimilar Structures; Spot-Weld Joint; Finite Element Analysis; Finite Element Model Updating; Response Surface Methodology*

Introduction

The evolution of current manufacturing technologies has emphasized the increasing utilization of heterogeneous materials across various sectors, including the aerospace and automotive industries [1]-[2]. Spot welding is a prevalent joining method, particularly in the automotive, aerospace, and electronics industries, where the fusion of dissimilar materials is crucial. A multitude of studies have underscored the advantages of employing a variety of materials in a specific structure, such as weight reduction, enhanced fuel efficiency, and improved mechanical properties of the structures [3]-[5]. However, the attainment of optimal spot welds for dissimilar materials presents a substantial challenge due to the disparities in the physical and chemical properties of the materials involved. Several studies have indicated that the task of seamlessly integrating multiple materials in spot welding is intricate due to the variation in the physical attributes, properties, and thermal expansion coefficients [6]-[7]. This has prompted investigations into the welding parameters that affect joint quality, such as current, pressure, and welding time [8]-[10].

Conversely, Finite Element Modeling (FEM) of spot welding on dissimilar materials serves as a valuable instrument for simulating and analyzing the properties and effects on the materials being joined. Considering that experimental testing of breaking hundreds of welds to comprehend their behavior is both labor-intensive and costly, models to predict the behavior of spot welds have been under development for several decades [11]. It is imperative to generate detailed simulations that can forecast the behavior of welded joints under various conditions. Nevertheless, numerous studies have underscored the limitations of constructing a reliable model. Dancette et al. [12] highlighted the inability to simulate the crack paths of a spot-welded dissimilar structure and to accurately locate the stress concentration. Mirmahdi [13] in his research also observed that there are

numerous factors to consider during the modeling of a spot-welded joint and that errors during simulation are unavoidable.

Numerous studies have indicated that the complexity of FEM for spot welding of dissimilar materials arises from the need to accurately represent the diverse thermal and mechanical properties of the materials involved, including their interactions during the welding process [14]-[15]. Various researchers have elaborated on how the differences in thermal conductivity, electrical resistivity, and mechanical strength of dissimilar materials can significantly impact the heat distribution, cooling rates, and resulting microstructures within the weld zone [16]-[17]. These factors introduce complexity to the accurate prediction of weld quality and performance.

Moreover, a prior study highlighted that the geometric accuracy of the models, the quality of the mesh, and the precision of boundary conditions all play crucial roles in the reliability of the simulation outcomes [15]-[18]. Another study emphasized the importance of high-quality meshing, particularly in regions with steep gradients like the heat-affected zones. This is because incorrect mesh configurations can lead to substantial inaccuracies in the results [19]. Therefore, optimizing the constructed finite element model can enhance the overall quality and performance of the simulations. A reliable simulation will contribute to a better understanding of the characteristics of spot welding, thereby improving the performance and durability of the constructed welded joint.

In recent developments, the technique of model updating, which fine-tunes a computational model to more accurately reflect experimental data and enhance the model's predictive capability, has been introduced to address these challenges [20]-[22]. Findings from these previous studies have confirmed that model updating enhances the predictive capability of simulations and provides a deeper insight into the changes in properties of spot welding dissimilar materials. On the other hand, the Response Surface Method (RSM) is a statistical technique used for developing, improving, and optimizing processes, providing a structured method to assess the relationships between multiple explanatory variables and one or more response variables [23]. In several studies, researchers have demonstrated that the application of model updating and RSM can provide a powerful approach to address the challenges associated with spot welding of dissimilar materials [24]-[27]. By using both techniques, researchers can achieve more accurate simulations leading to better optimization of welding parameters. This not only enhances the quality of welded joints but also reduces the need for extensive experimental testing, thereby saving time and resources.

This research aims to enhance the finite element model of dissimilar plates joined by spot welding through input property optimization. The methodology involves updating the constructed FE model and optimizing parameters using RSM. The comparative analysis of these methods is anticipated to identify the most reliable approach for developing a high-

quality FE model. Essentially, this study offers an integrated solution for optimizing the spot-welding process for dissimilar materials, potentially improving manufacturing quality and efficiency across various sectors.

FEMs and Experimental Modal Analysis for Spot-Welded Joints

FE models

A dissimilar plate structure with Resistance Spot-Welded (RSW) joints was studied in this work. A variety of modeling approaches for spot weld joints were developed, incorporating different element types such as shell elements, beam elements, and solid elements. These models were constructed using MSC PATRAN, a commercial FEA software. Consequently, three unique modeling approaches were established: CBAR, CBEAM, and CWELD joining. CBAR elements are ideal for modeling slender, straight structures like simple beams and trusses. CBEAM elements provide advanced modeling for beams of any shape with variable cross-sections, suitable for complex structures. CWELD elements simulate welds between components, capturing stiffness and load transfer, and are commonly used in the automotive and aerospace industries. Numerous studies have been conducted on the FEA of dissimilar plate structures with spot-welded joints [14], [19], [28]. In relation to the spot-welded joints, this study opted to focus on the CWELD connector to emulate the actual structure. Figure 1 depicts the FE model of the dissimilar plate structure with spot-welded joints, represented by the CWELD connector. The structure consists of two distinct plates, specifically the AL7075 plate and the AL6061 plate, which are interconnected using a total of ten weld connectors. All plates have identical dimensions, with a length, width, and thickness of 200 mm, 200 mm, and 2 mm, respectively. The overlap width between the two plates measures 20 mm.

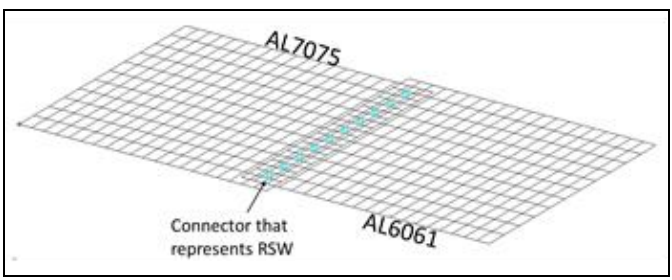

Figure 1: The FE model of the plate structure

The FE model of the dissimilar plate structure with joining was developed using PATRAN software, as depicted in Figure 2. This study employed QUAD4 shell elements to simulate the plate structure, involving a total of 440 elements and 504 nodes. The elements used for the plate structure were 1 mm in dimension and were of the 2D shell element type. The constructed model had an overall length of 380 mm, with a 5 mm gap at the overlap point. The material properties applied in the FE model are detailed in Table 1.

The study utilized the SOL103 solution sequence to emulate free-free boundary conditions, ensuring that no load, translational, or rotational boundary conditions were imposed on any node within the system [29]. The CWELD approach employed two grid points to enhance the rigidity of the six degrees of freedom associated with each grid point. The elastic axis and shear center of the CWELD were found to coincide.

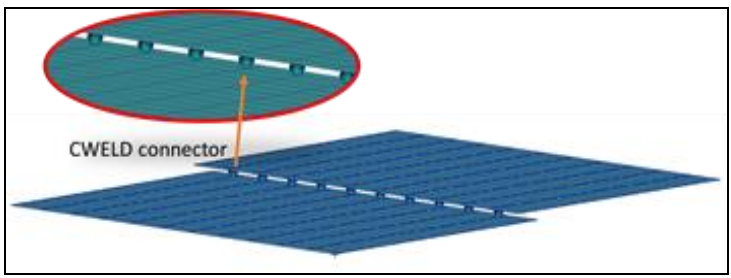

Figure 2: The CWELD connector of the plate structure

Table 1: Material properties for structure

Properties	Plate A (AL7075)	Plate B (AL6061)	Unit
Young's modulus, *E*	71.7	68.9	GPa
Poisson ratio, ν	0.33	0.33	-
Density, ρ	2810	2700	kg/m^3

EMA for data correlation

A test system was constructed for the free modal analysis of a dissimilar plate structure, as depicted in Figure 3. The plate, which is spot-welded at the center (overlap), was examined using a roving impact hammer and two uni-axial accelerometers to assess its dynamic characteristics. The experimental apparatus for the EMA comprised ME's Scope VES, a Data Acquisition System (NI DAQ), an impact hammer, and a uni-axial accelerometer, as illustrated in Figure 4. The EMA was performed on a dissimilar plate structure with a nominal thickness of 2 mm and dimensions of 380 mm x 200

mm. The materials used in this study were different series of aluminum plates, specifically AL6061 and AL7075.

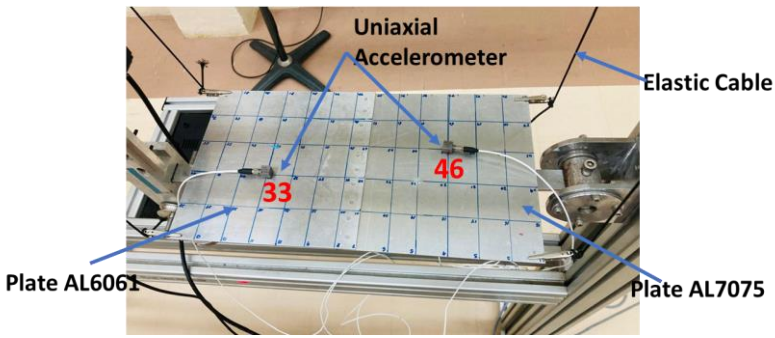

Figure 3: The experimental modal analysis setup of the plate

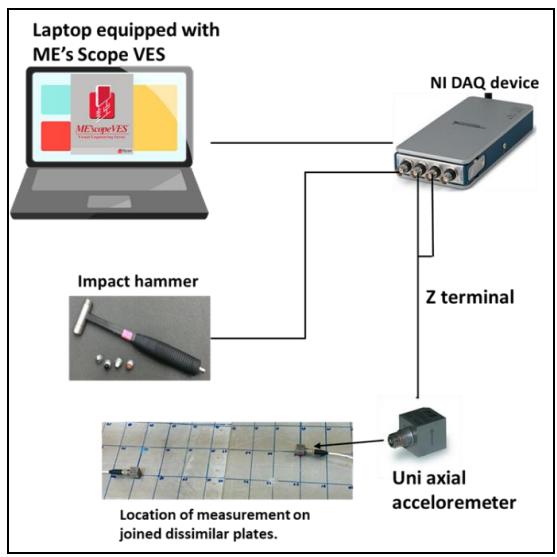

Figure 4: Tools and instruments used in experimental modal analysis

The plate was discretized into 84 elements to determine the optimal number and placement of measurement points. The number of elements was estimated based on the modal characteristics of the plate, derived from finite element analysis. The dissimilar plate was hanging from the test rig using an elastic cable to simulate the free-free boundary condition. In this study, measurement points 33 and 46 were identified as fixed excitation points.

Using wax, the acceleration sensors were affixed to the measurement points on the experimental plate. Given the dissimilar nature of the plate structure, it was deemed sufficient to place two sensors on each plate to capture the required mode shapes. The natural frequencies and mode shapes extraction was conducted using the curve fitting approach implemented in the ME's Scope VES software.

Correlation analysis

In this study, the ideal value of error is zero, indicating a perfect correlation between the test modal frequency and the calculated frequency. Any deviation from zero signifies a discrepancy between these two frequencies. Three types of connectors, used to simulate weld joints, were evaluated against benchmark values derived from EMA. The percentage errors of the CBAR model, CBEAM model, and CWELD model were compared to those of EMA, as detailed in Table 2. Both the CBAR and CBEAM models exhibited the lowest average percentage error of 5.66%. In contrast, the CWELD model showed the highest average error percentage at 6.87%. Additionally, the error percentage for the natural frequency at mode NF3 was found to be the highest among all modes across all three models.

Table 2: Natural Frequency of FEA correlate with EMA data

Mode	Natural Frequency (Hz)						
	EMA	**CBAR**	**Error %**	**CBEAM**	**Error %**	**CWELD**	**Error %**
NF1	94.28	85.82	8.97	85.82	8.97	105.28	11.67
NF2	185.6	176.88	4.70	176.89	4.69	180.35	2.83
NF3	272.8	305.63	12.03	305.66	12.05	313.39	14.88
NF4	314.6	321.91	2.32	321.92	2.33	327.06	3.96
NF5	451.2	491.25	8.88	491.33	8.89	510.92	13.24
NF6	635.2	641.72	1.03	641.76	1.03	634.59	0.10
NF7	746	758.39	1.66	758.41	1.66	756.75	1.44
Total average error			5.66		5.66		6.87

These discrepancies can be attributed to various factors, including uncertainties in material properties, geometric imperfections, and the presence of manufacturing defects. These factors significantly influence the structural stiffness and damping characteristics of lightweight structures [30]. Additionally, EMA measurements may be affected by numerous ambient factors, the setup of the testing apparatus, and inherent limitations in the instrumentation used.

Despite exhibiting the highest percentage error, the CWELD models were found to possess suitable parameters for model updating in welded modeling. This is because these models accurately represent spot welds in the EMA test structure, as discussed in a previous section. Their utility lies in

their enhanced accuracy in predicting the dynamic behavior of real structures. To improve the correlation between numerical predictions and measured equivalents of bolted models, the CWELD model was utilized for Finite Element Model Updating (FEMU).

FEMU and RSM

Updating model and modal properties

FEMU techniques are deliberate to enhance the reliability of analytical analyses. After identifying the sensitive parameters through a sensitivity analysis, the model updating process was initiated. This process updated the predicted values from FEA with measured values obtained from EMA. The updated values were achieved by correcting less accurate property definitions into more optimized values [31]. In this research, four parameters were chosen for the sensitivity analysis. These include Young's modulus for both the plate materials, E_{AL7075}, E_{AL6061}, and the connector, $E_{CWELD,}$ as well as the diameter of the connector, D_{CWELD} as depicted in Figure 5.

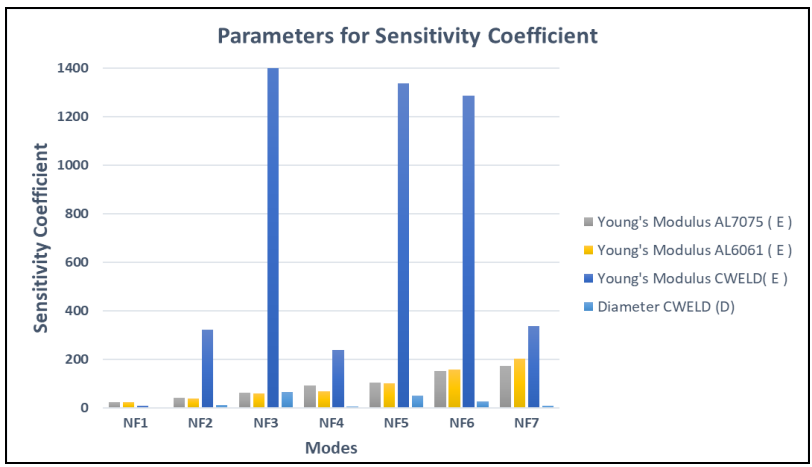

Figure 5: Parameters for sensitivity coefficient

Table 3 presents the variations in updated values compared to the initial values for the selected parameters, as affected by the design variable. The table reveals that the changes in Young's modulus for both plate structures and the diameter of the joining element demonstrate a greater sensitivity compared to Young's modulus of the joining element. This is largely due to the assumptions made within the simulation software. In many simulation situations, the setting of upper and lower limits is done based on

certain assumptions to preserve the accuracy of the simulation [32]. Specifically, for joining simulations, it is common practice to assign higher values to Young's modulus. This increases the stiffness of the element or decreases its deformability.

Table 3: Changes in parameter value based on the design variable

Parameter	Initial value (i)	Updated value (u)	Unit	Changes $\|(u-i)/i\|$
Young's modulus AL7075 (E_{AL7075})	71.7	70.27	GPa	0.02
Young's modulus AL6061 (E_{AL6061})	68.9	69.45	GPa	0.008
Young's modulus CWELD (E_{CWELD})	1000	100	GPa	0.9
Diameter CWELD (D_{CWELD})	10	9.6	mm	0.04

The findings presented in Table 4 demonstrate that applying FEMU techniques effectively updated the natural frequencies. However, it's important to note that the accuracy of the updated results varied. All seven modes derived from the initial FE model were successfully calibrated based on the empirical data collected. The improvement in adjustment is evident in column VI, where the total average error of the initial FE decreased from 6.87% (column IV) to 4.04%. This indicates an improvement in simulation value accuracy by nearly 41% from the initial value.

Table 4: Updated correlation of natural frequencies for CWELD models

Mode (I)	Natural Frequency (Hz)				
	EMA (II)	Initial CWELD (III)	Error (%) (IV)	Updated CWELD SOL200 (V)	Error (%) (IV)
NF1	94.28	105.28	11.67	88.54	6.09
NF2	185.6	180.35	2.83	169.85	8.49
NF3	272.8	313.39	14.88	279.47	2.45
NF4	314.6	327.06	3.96	328.71	4.49
NF5	451.2	510.92	13.24	444.35	1.52
NF6	635.2	634.59	0.10	649.91	2.32
NF7	746	756.75	1.44	768.06	2.96
Total average error			6.87		4.04

The third and fifth modes, NF3 and NF5, showed the most significant accuracy, with error reductions of nearly 83% and 88%, respectively from the initial error percentage. This was followed by the first mode, NF1, which

showed a reduction of 48% from the initial value. The second mode, NF2, exhibited the highest inaccuracy, with the percentage of error increasing by 5.66% from the initial percentage error. This inaccuracy in NF2 could be due to several factors such as limitations in modeling, uncertainties in parameters, and errors in measurement or numeric that could arise from measurement techniques or model equation discretization for this mode. In this study, it will be necessary to compare the results with the RSM to determine the most effective technique for reducing the discrepancy error in this specific structure [33].

Analysis of RSM

Four numerical factors were pinpointed for subsequent optimization using RSM as input parameters. These encompass A: Young's modulus AL7075 (E_{AL7075}), B: Young's modulus AL6061 (E_{AL6061}), C: Young's modulus CWELD (E_{CWELD}), and D: diameter of CWELD connector (D_{CWELD}). Each of these parameters underwent a three-level factorial design, incorporating variations at low, medium, and high levels, as outlined in Table 5.

Table 5: Level of parameter variables

Parameter	Codes	Levels			Unit
		Low	Medium	High	
Young's modulus AL7075 (E_{AL7075})	A	69	72	75	GPa
Young's modulus AL6061 (E_{AL6061})	B	67	69	71	GPa
Young's modulus CWELD (E_{CWELD})	C	900	1000	1100	GPa
Diameter CWELD (D_{CWELD})	D	0.0023	0.0025	0.0027	m

In this study, the RSM was applied using Design Expert (DE) version 13, and the significance of the model and response analysis was determined using Analysis of Variance (ANOVA). ANOVA was used to evaluate the equality of the models developed for each response parameter. To ensure the reliability and accuracy of the results, it is suggested that all simulation results be subjected to an ANOVA approach, specifically using the Fisher test (F-test) [34]-[35]. A coefficient is considered statistically significant when the estimated probability is below the predetermined significance threshold of 0.05. This research relies on using the F-value, which represents the ratio of the mean square of the model regression to the mean square of the residual. For the analysis to be considered statistically significant, the F-value must exceed the critical value derived from the tabulated value of the F-distribution, based on a specific number of degrees of freedom within the

model. The correlation between the independent variables and the response variables was assessed through the visualization of response surface 3D plots.

A comprehensive assessment was conducted on the outcomes related to various response parameters. This included an in-depth review of the ANOVA results, with a particular emphasis on the F-value and p-value. The significance of the input variables on the output parameters was also evaluated. A p-value less than 0.05 signifies the importance of the variable parameter, while a p-value greater than 0.05 indicates its insignificance [36]-[37]. The size of the F-value serves as an indicator of the impact level of the variable parameter on the response parameter.

Table 6 outlines a variety of statistical parameters obtained from the developed models. Generally, a larger F-value in ANOVA signifies a more substantial disparity among sample means, while a smaller p-value equates to a higher degree of significance, offering strong support for the model's significance. The model's overall significance implies the importance of all responses. The results from Table 6 indicate that the model is significant across all response modes. The evaluation of the correlation coefficient (R^2), adjusted correlation coefficient (Adj. R^2), and predicted correlation coefficient (Pred. R^2) values is used to gauge the accuracy of the statistical results produced by RSM [38]-[39]. Notably, the R^2, Adj. R^2 and Pred. R^2 values for all the models are within an acceptable range, approaching 1. The magnitude of the R^2 value is considered a measure of the model's sufficiency and precision in forecasting the actual parameter value [40]. The slight difference between the R^2, Adj. R^2 and Pred. R^2 values, less than 0.2 indicates the models' adequacy.

Table 6: ANOVA for the response model

Response mode	Sum of squares	df	Mean square	F-value	p-value	Remarks
NF1	2815.08	6	469.18	219.42	< 0.0001	significant
NF2	286.48	6	47.75	3917.39	< 0.0001	significant
NF3	911.32	10	91.13	2687.40	< 0.0001	significant
NF4	1003.24	10	100.32	4514.20	< 0.0001	significant
NF5	2348.77	6	391.46	2335.31	< 0.0001	significant
NF6	3851.77	6	641.96	19016.14	< 0.0001	significant
NF7	6037.09	10	603.71	444.74	< 0.0001	significant

As shown in Table 7, the highest Adj. R^2 is recorded for Mode NF6, reaching 0.9993, while the lowest value is seen for Mode NF1, at 0.9425. Considering the correlation coefficient values for each response, the software autonomously opted for a quadratic model to forecast different natural frequency parameters for the dissimilar structure.

Table 7: ANOVA result for Pred. R^2 and Adj. R^2

Response mode	Std. Dev.	Mean	C.V.%	R^2	Adj. R^2	Pred. R^2
NF1	1.46	101.89	1.44	0.9468	0.9425	0.9362
NF2	0.1104	180.54	0.0611	0.9969	0.9966	0.9962
NF3	0.1841	313.06	0.0588	0.9974	0.9970	0.9965
NF4	0.1491	327.85	0.0455	0.9985	0.9982	0.9979
NF5	0.4094	511.36	0.0801	0.9947	0.9943	0.9937
NF6	0.1837	659.34	0.0279	0.9994	0.9993	0.9992
NF7	1.17	767.88	0.1517	0.9845	0.9823	0.9793

Table 8 presents the importance of model terms, as determined by the ANOVA results obtained from the quadratic model for each response. A detailed analysis of the table shows that both E_{AL7075} (A), E_{AL6061} (B), and D_{CWELD} (D) have a significant effect on all parameters, while E_{CWELD} (C) is not significant for all responses. Interestingly, the interaction effect between both of Young's modulus plates has had a noticeable impact on 3 responses, namely Mode NF3, Mode NF4, and Mode NF7, indicating a satisfactory significance within the context of this study. The significance of the results is gauged by the p-values derived from the software, where a p-value less than 0.05 or within the 95% confidence interval signifies the importance of the model terms, while a p-value greater than 0.05 implies insignificance [41]. In summary, these findings collectively imply that E_{CWELD}, referred to as the joining component, does not make a significant contribution to the overall structural model.

Table 8: ANOVA results for the significance of model terms

Response (mode)	A	B	C	D	AB
NF1	✓	✓	x	✓	x
NF2	✓	✓	x	✓	x
NF3	✓	✓	x	✓	✓
NF4	✓	✓	x	✓	✓
NF5	✓	✓	x	✓	x
NF6	✓	✓	x	✓	x
NF7	✓	✓	x	✓	✓

✓ - Significant at 95% confidence interval, x - not significant at 95% confidence interval

Mathematical models for all responses have been developed to predict the respective natural frequency values, taking into account the various input parameters as detailed in Equations (1) to (7).

NF1 = 101.89 + (-0.7230) * E_{AL7075} + (-0.2278) * E_{AL7075} + (1.29) * E_{AL6061} + 0.2970 * E_{AL6061} + (-8.05) * D_{CWELD} + 2.85 * D_{CWELD} (1)

NF2 = 180.54 + (-1.89) * E_{AL7075} + (-0.0285) * E_{AL7075} + (-1.30) * E_{AL6061} + 0.0193 * E_{AL7075} + (-0.1348) * D_{CWELD} + 0.0507 * D_{CWELD} (2)

NF3 = 313.06 + (-3.41) * E_{AL7075} + 0.3967 * E_{AL7075} + (-2.47) * E_{AL6061} + 0.2341 * E_{AL6061} + (-0.6052) * D_{CWELD} + 0.0785 * D_{CWELD} + 0.95 * (E_{AL7075})(E_{AL6061}) + (-0.1148) * (E_{AL7075})(E_{AL6061}) + (-0.0559) * (E_{AL7075})(E_{AL6061}) + 0.0726 * (E_{AL7075})(E_{AL6061}) (3)

NF4 = 327.85 + (-3.23) * E_{AL7075} + (-0.41) * E_{AL7075} + (-2.3) * E_{AL6061} + (-01419) * E_{AL6061} + (-0.8048) * D_{CWELD} + 0.1867 * D_{CWELD} + (-0.8044) * (E_{AL7075})(E_{AL6061}) + (-0.0256) * (E_{AL7075})(E_{AL6061}) + (-0.0115) * (E_{AL7075})(E_{AL6061}) + (-0.0048) * (E_{AL7075})(E_{AL6061}) (4)

NF5 = 511.36 + (-5.3) * E_{AL7075} + (-0.0921) * E_{AL7075} + (-3.8) * E_{AL6061} + 0.0616 * E_{AL6061} + (-0.9414) * E_{CWELD} + 0.2494 * E_{CWELD} (5)

NF6 = 659.34 + (-6.85) * E_{AL7075} + (-0.0425) * E_{AL7075} + (-4.83) * E_{AL6061} + 0.0342 * E_{AL6061} + (-1.06) * E_{CWELD} + 0.2001 * E_{CWELD} (6)

NF7 = 767.88 + (-7.25) * E_{AL7075} + (-1.77) * E_{AL7075} + (-5.26) * E_{AL6061} + (-0.5453) * E_{AL6061} + (-2.08) * E_{CWELD} + 0.6091 * E_{CWELD} + (-3.84) * (E_{AL7075})(E_{AL6061}) + 0.5105 * (E_{AL7075})(E_{AL6061}) + 0.3072 * (E_{AL7075})(E_{AL6061}) + (-0.7891) * (E_{AL7075})(E_{AL6061}) (7)

Figure 6 depicts the relationship between the forecasted and actual values of the parameters, providing a comparison between the FEA and RSM response parameters. Most of the data points are seen near the fit line, signifying a robust correlation between the real and predicted values. The correlation coefficient values for various parameters indicate the effectiveness of the established model in forecasting the natural frequency, based on the chosen material parameters for the heterogeneous plate structure. A closer look at the figure shows that Mode NF3, Mode NF4, Mode NF6, and Mode NF7 are located nearer to the line, exhibiting a stronger correlation compared to the remaining three responses. This observation further underscores the appropriateness of these models for the

FE data, facilitating the analysis and prediction of the natural frequency performance.

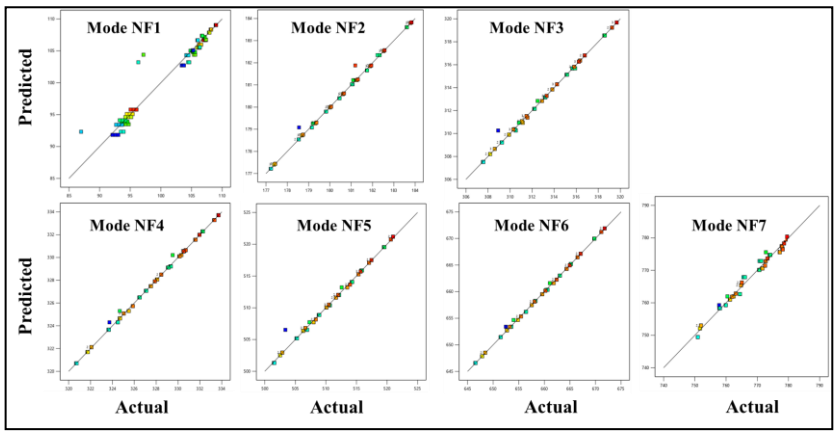

Figure 6: Comparison of FEA and RSM response parameters

The influence of various factors is demonstrated through three-dimensional (3D) response surface plots and segmented data plots, as shown in Figure 7 to Figure 9. The 3D response surface curve aids in the mutual understanding of variable parameters, assisting in identifying the optimal level for each variable to achieve the maximum mode response in the natural frequency. Additionally, the graphs in Figure 7 to Figure 9 help in determining the most effective range for all four variable factors. It is clear from the figures that an increase in Young's modulus for both plate structures leads to an increase in the natural frequency.

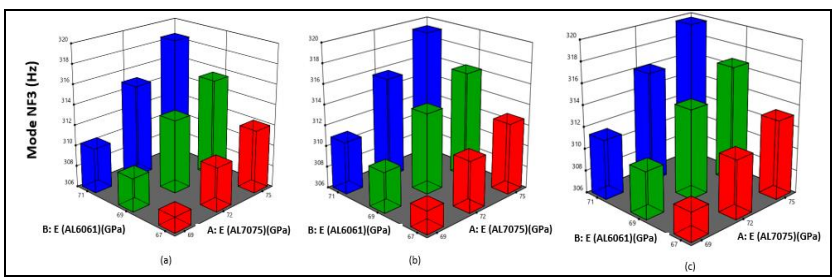

Figure 7: Response surface 3D plots effect of E_{AL7075} and E_{AL6061} variables of Young modulus's connector and diameter connector for NF3

Considering the findings in Table 8, our discourse primarily revolves around three responses for the 3D response surface, namely mode NF3, NF4, and NF7. In Figure 7, the influence of Young's modulus for both heterogeneous plates is more pronounced in the alterations of natural frequency, as illustrated in Figure 7(a), relative to the interactions between the Young's modulus connector and the diameter connector based on the lower boundary from E_{CWELD} and D_{CWELD}, Figures 7(b) based on middle boundary of E_{CWELD} and D_{CWELD} and Figures 7(c) based on the upper boundary of E_{CWELD} and D_{CWELD}. The maximum natural frequency value of 319.67 Hz is prominently seen in Figure 7(c), with a variation in the value of nearly 3 Hz, while the changes are relatively stable for both of the other interactions.

Additionally, as depicted in Figure 8 and Figure 9, the same interaction effect as described in Figure 7 is also utilized. The highest peak of the natural frequency value is noted in Figure 8(c), achieving 333.71 Hz, with a variation in the value of approximately 6 Hz, while the changes in the interactions are comparatively more modest, at 3.2 Hz and 3 Hz, respectively. The unique modes of natural frequency, characterized by specific material properties, have profound impacts on the update procedure in FE analysis. This assists in portraying the real structure accurately and contributes to reducing the influence of vibrations in structures with less weight. This is crucial in academic writing to avoid plagiarism.

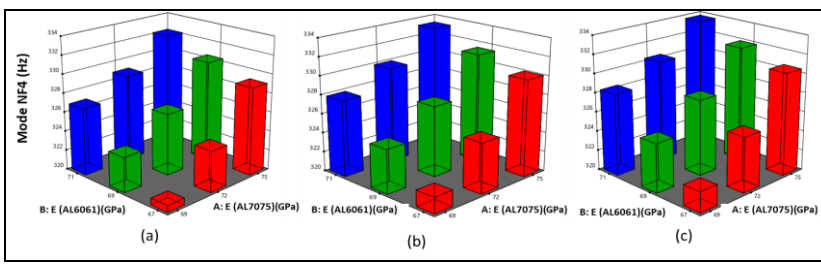

Figure 8: Response surface 3D plots effect of E_{AL7075} and E_{AL6061} variables of Young modulus's connector and diameter connector for NF4

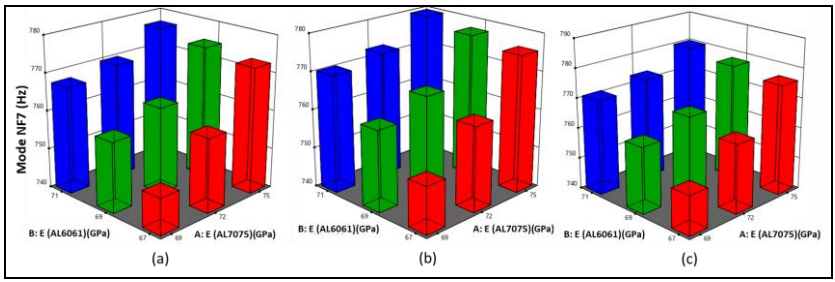

Figure 9: Response surface 3D plots effect of E_{AL7075} and E_{AL6061} variables of Young modulus's connector and diameter connector for NF7

Optimization of RSM

The optimization process was carried out using RSM, considering both input and output response parameters. The input parameters included Young's modulus of AL7075, AL6061, CWELD, and the diameter of the joining CWELD. The approach, along with the lower and upper limit values of the input and response parameters, and the optimized parameter value, are presented in Table 9. During the optimization, RSM was used to establish the lower and upper limits of the parameters. In the approach section, the minimum and range values targeted in the response parameters were inputted. The goal was to maximize the effectiveness of the natural frequency value for the lightweight plate structure. For all the main factors, a range approach was selected, while a minimized target was chosen for all the mode responses.

Table 9: Criteria and results of optimization

Parameter	Target	Lower Limit	Upper Limit	Optimized input and response parameter	Unit
A: E_{AL7075}	In range	69	75	69	GPa
B: E_{AL6061}	In range	67	71	67	GPa
C: E_{CWELD}	In range	900	1100	900	GPa
D: D_{CWELD}	In range	0.005	0.015	0.005	m
Mode NF1	Minimize	86.99	109.03	91.820	Hz
Mode NF2	Minimize	177.22	183.83	177.22	Hz
Mode NF3	Minimize	307.54	319.67	307.52	Hz
Mode NF4	Minimize	320.68	333.71	320.70	Hz
Mode NF5	Minimize	501.48	521	501.32	Hz
Mode NF6	Minimize	646.5	671.79	646.59	Hz
Mode NF7	Minimize	750.93	779.54	749.44	Hz

The optimization's precision is represented by the desirability rate, which was found to be 0.972. The closeness of this value to 1 reinforces the

appropriateness of the performed optimization [42]. Following the optimization, the ideal input parameters were identified as 69 GPa for Young's modulus AL7075, 67 GPa for Young's modulus AL6061, 900 GPa for Young's modulus CWELD, and a 0.005 m diameter for the connector CWELD. Based on these optimal input parameters, all responses were observed to align closely with the targeted minimum values.

Optimization results between FEMU and RSM

The comparative analysis of the two methodologies, aimed at minimizing the discrepancy between experimental and computational data, reveals a notable reduction in the percentage error from the initial CWELD value, as illustrated in Table 10. The optimization process utilizing SOL200 also referred to as FEMU, results in the lowest percentage error of 4.04%. In contrast, the optimization using RSM leads to a marginally higher percentage error of 5.02%. Despite this difference, the study successfully fulfils its objective of evaluating the efficacy of both optimization methods in reducing the error disparity within the lightweight dissimilar structure.

Moreover, the noticeable differences in the optimization procedures can be traced back to the trial-and-error method used in defining boundaries for model updating, whereas, for RSM, the levels are determined based on forecasts derived from the values used in FEA. In essence, the comparison highlights the successful application of both optimization techniques in reducing errors. While model updating can provide superior precision in defining boundaries, it cannot create mathematical models, a vital attribute offered by RSM in the optimization process.

Table 10: Optimization of natural frequencies for CWELD models

Mode	Natural Frequency (Hz)						
	EMA	**Initial CWELD**	**Error %**	**Updated CWELD (SOL200)**	**Error %**	**Optimization CWELD (RSM)**	**Error %**
NF1	94.28	105.28	11.67	88.54	6.09	91.82	2.61
NF2	185.6	180.35	2.83	169.85	8.49	177.22	4.52
NF3	272.8	313.39	14.88	279.47	2.45	307.52	12.73
NF4	314.6	327.06	3.96	328.71	4.49	320.70	1.94
NF5	451.2	510.92	13.24	444.35	1.52	501.32	11.11
NF6	635.2	634.59	0.10	649.91	2.32	646.59	1.79
NF7	746	756.75	1.44	768.06	2.96	749.44	0.46
Total average error			6.87		4.04		5.02

Conclusion

This research focused on the analysis and exploration of improving dynamic properties for the union of different plate structures. A variety of conditions were taken into account during the execution of experimental and simulation tests, including factors like Young's modulus for both AL7075 and AL6061 plates, the joining CBAR, and the diameter of the CWELD connector. The measurement of all material property parameters led to the creation of a mathematical method that correlates these parameters with the factors under consideration. The results of the study indicate a significant interrelation among the four factors, especially in the case of Young's modulus plates, specifically $E_{AL}7075$ and $E_{AL}6061$. The findings from FEMU reveal that all four factors play a significant role in error reduction, while RSM shows that only three factors are significant in reducing the error of natural frequency. Both optimization methods are effective in reducing discrepancy errors and provide unique benefits in the optimization process. These methods can be robust solutions for tackling multi-objective optimization challenges in dynamic properties parameter optimization.

Contributions of Authors

The authors confirm the equal contribution in each part of this work. All authors reviewed and approved the final version of this work.

Funding

This work received financial support under Fundamental Research Grant Scheme No. FRGS/1/2021/TK0/UMP/02/69.

Conflict of Interests

All authors declare that they have no conflicts of interest.

Acknowledgment

The authors would like to thank the Ministry of Higher Education for providing financial support under Fundamental Research Grant Scheme No. FRGS/1/2021/TK0/UMP/02/69 (University reference RDU 210124) and Universiti Malaysia Pahang Al-Sultan Abdullah for laboratory facilities.

References

[1] S. Kumari, E. K. Rao Patro, S. Singh, P. K. Chandra, S. A. Kareem, and L. Kansal, "Advanced welding of dissimilar materials for aerospace and automotive applications," *E3S Web of Conferences*, vol. 430, pp. 1-9, 2023.

[2] T. Sun, C. Liu, P. Franciosa, N. Freguson, G. Gibbons, D. Ceglarek, E. Mogire, and P. Zhang, "Effect of placement configuration on the microstructure, porosity and mechanical performance of dissimilar remote laser welding of additive manufactured AlSi10Mg alloy and conventionally manufactured 1050 aluminium sheet," *Journal of Materials Research and Technology*, vol. 27, pp. 5639-5650, 2023.

[3] S. A. Khan, H. Liaqat, F. Akram, and H. Ali Khan, "Development of a design space for dissimilar materials joining in aerospace applications," *The Aeronautical Journal*, vol. 128, pp. 1-18, 2023.

[4] Wei, C. and L. Li, "Recent progress and scientific challenges in multi-material additive manufacturing via laser-based powder bed fusion", *Virtual and Physical Prototyping*, vol. 16, no. 3, pp. 347-371, 2021.

[5] Chowdhury, I.D., et al., "Investigation of mechanical properties of dissimilar joint of 6063 aluminium and C26000 copper alloy by friction stir welding," *Materials Today: Proceedings*, vol. 44, pp. 4039-4047, 2021.

[6] I. Chowdhury, S. Kaushik, M. Kaustav. Kumar, R. Swapna, and G. Sujit, "Investigation of mechanical properties of dissimilar joint of Al6063 aluminium alloy and C26000 copper alloy by ultrasonic assisted friction stir welding," *Materials Today: Proceedings*, vol. 50, pp. 1527-1534, 2021.

[7] Shinjo, J. and C. Panwisawas, "Chemical species mixing during direct energy deposition of bimetallic systems using titanium and dissimilar refractory metals for repair and biomedical applications", *Additive Manufacturing*, vol. 51, pp. 1-13, 2022.

[8] D. Mishra, K. Rajanikanth, M. Shunmugasundaram, A. Praveen Kumar, and D. Maneiah, "Dissimilar resistance spot welding of mild steel and stainless steel metal sheets for optimum weld nugget size," *Materials Today: Proceedings*, vol. 46, pp. 919-924, 2021.

[9] Suryanarayanan, R. and V. Sridhar, "Experimental investigation on the influence of process parameters in Friction stir spot welded dissimilar aluminum alloys," *Materials Today: Proceedings*, vol. 27, pp. 529-533, 2020.

[10] I. Renreng Ariyanto, H. Arsyad, and M. Abdul Syahid, "Optimization parameter resistance spot welding dissimilar material-a review," *AIP Conference Proceedings*, vol. 2630, no. 1, pp. 1-9, 2023.

[11] A. Mohamadizadeh, E. Biro, and M. Worswick, "Novel double-half spot weld testing technique for damage progress and failure analysis

using digital image correlation techniques", *Experimental Mechanics*, vol. 61, no. 9, pp. 1405-1418, 2021.
[12] S. Dancette, H. Thibaut, T. Dupuy, and D. Fabregue, "Finite element modeling of deformation and fracture of advanced high strength steels dissimilar spot welds", *Engineering Fracture Mechanics,* vol. 258, pp. 1-34, 2021.
[13] E. Mirmahdi, "Numerical and experimental modeling of spot welding defects by ultrasonic testing on similar sheets and dissimilar sheets," *Russian Journal of Nondestructive Testing,* vol. 56, pp. 620-634, 2020.
[14] R. Pramod, M. K, Subramaniyan, R. Kannan Arasappan, and N. Siva Shanmugam, "Resistance spot-welded dissimilar sheets—parametric behavioral analysis using experimentation and simulation", *Transactions of the Indian Institute of Metals,* vol. 75, no. 5, pp. 1309-1328, 2022.
[15] A. Arumugam, and A. Pramanik, "Review of experimental and finite element analyses of spot weld failures in automotive metal joints," *Jordan Journal of Mechanical & Industrial Engineering,* vol. 14, no. 3, pp. 315-337, 2020.
[16] K. Manuel Prabitz, M. Pichler, T. Antretter, H. Schubert, B. Hilpert, M. Guruber, R. Sierlinger, and W. Ecker, "Validated multi-physical finite element modelling of the spot welding process of the advanced high strength steel dp1200hd", *Materials*, vol. 14, no. 18, pp. 1-19, 2021.
[17] J. Gutierrez Moreno, J. Ciao, M. Fronzi, and M. H. N. Assadi, "A review of recent progress in thermoelectric materials through computational methods", *Materials for Renewable and Sustainable Energy,* vol. 9, no. 3, pp. 1-22, 2020.
[18] N. Abdullah, M. Asri, and M. S. M. Sani, "Strategies of finite element modeling for spot welded joints and its modal correlation with experimental data," *International Journal of Automotive and Mechanical Engineering*, vol. 19, no. 1, pp. 9543-9550, 2022.
[19] R. S. Tabar, K. Wärmefjord, and R. Söderberg, "A new surrogate model–based method for individualized spot welding sequence optimization with respect to geometrical quality," *The International Journal of Advanced Manufacturing Technology,* vol. 106, no. 5, pp. 2333-2346, 2020.
[20] J. E. Mottershead, and M. I. Friswell, "Model updating in structural dynamics: A survey," *Journal of Sound and Vibration*, vol. 167, no. 2, pp. 347-375, 1993.
[21] M. S. M. Sani, N. A. Nazri, M. N. Abdul Rani, and M. A. Yunus, "Dynamic analysis of I cross beam section dissimilar plate joined by TIG welding," *AIP Conference Proceedings*, vol. 19252, pp. 1-8, 2018.
[22] Başağa, H.B., T. Türker, and A. Bayraktar, "A model updating approach based on design points for unknown structural parameters", A*pplied Mathematical Modelling*, vol. 35, no. 12, pp. 5872-5883, 2011.

[23] G. H. Farrahi, K. R. Kashyzadeh, M. Minaei, A. Sharifpour, and S. Riazi, "Analysis of resistance spot welding process parameters effect on the weld quality of three-steel sheets used in automotive industry: Experimental and finite element simulation," *International Journal of Engineering*, vol. 33, no. 1, pp. 148-157, 2020.

[24] W. W. I. Wan Iskandar Mirza, M. N. Abdul Rani, M. A. Yunus, and B. Athikary, "Correlating finite element model of a car spot-welded front-end module in the light of modal testing data," *International Journal of Automotive and Mechanical Engineering*, vol. 17, no. 2, pp. 7974-7984, 2020.

[25] P. Nagasai, A. Ramaswamy, S. Malarvizhi, V. Balasubramanian, and M. Dwivedy, "Optimization of process parameters of cold metal transfer arc welding of AA 6061 Aluminium Alloy-AZ31B magnesium alloy dissimilar joints using response surface methodology," *International Journal of Lightweight Materials and Manufacture*, vol. 7, no. 5, pp. 738-752, 2024.

[26] Md Khaliz Mumtaz, "Study and analysis of spot welding of dissimilar material 1008 low carbon steel 5052 aluminum alloy," *International Journal For Research In Applied Science and Engineering Technology*, vol. 8, pp. 1-17, 2020.

[27] S. Chakraborty, and A. Sen, "Adaptive response surface based efficient finite element model updating", *Finite Elements in Analysis and Design*, vol. 80, pp. 33-40, 2014.

[28] R. S. Tabar, S. Lorin, C. Cromvik, L. Lindkvist, K. Wärmefjord, and R. Söderberg, "Efficient spot welding sequence simulation in compliant variation simulation," *Journal of Manufacturing Science and Engineering*, vol. 143, no. 7, pp. 1-10, 2021.

[29] R. A. Méndez-Sánchez, and A. A. Fernández-Marín, "Analytical solutions for the Timoshenko beam theory with free-free boundary conditions," *arXiv preprint arXiv:*2104.14128, pp. 1-14, 2021.

[30] C. A. Geweth, S. K. Baydoun, F. Saati, K. K. Sepahvand, and S. Marburg, "Effect of boundary conditions in the experimental determination of structural damping", *Mechanical Systems and Signal Processing*, vol. 146, pp. 1-8, 2021.

[31] S. Ereiz, I. Duvnjak, and J. Fernando Jiménez-Alonso, "Review of finite element model updating methods for structural applications", *Structures*, vol. 41, pp. 684-7223, 2022.

[32] S. Zak, C. O. W. Trost, P. Keriml, and M. Cordill, "Accurate measurement of thin film mechanical properties using nanoindentation," *Journal of Materials Research*, vol. 37, no. 7, pp. 1373-1389, 2022.

[33] Reji, M. and R. Kumar, "Response surface methodology (RSM): An overview to analyze multivariate data," *Indian Journal of Microbiology Research*, vol. 9, no. 4, pp. 241-248, 2022.

[34] S. Balti, A. Boudenne, and N. Hamdi, “Characterization and optimization of eco-friendly gypsum materials using response surface methodology,” *Journal of Building Engineering*, vol. 69, pp. 106219-10621, 2023.

[35] M. Babagiray, S. M. Safieddin Ardebili, E. Aytav, O. Can, and A. A. Boroiu, “Multi-objective optimization of DI diesel engine performance and emission parameters fueled with Jet-A1 – Diesel blends”, *Energy*, vol. 242, no. 5, pp. 122997, 2022.

[36] X. Feng, Y. Liu, X. Li, and H. Liu “RSM, ANN-GA and ANN-PSO modeling of SDBS removal from greywater in rural areas via Fe2O3-coated volcanic rocks”, *RSC Advances*, vol. 12, no. 10 pp. 6265-6278, 2022.

[37] J. Anani, H. Noby, A. Zkria, T. Yoshitake, M. Elkady, “Monothetic analysis and response surface methodology optimization of calcium alginate microcapsules characteristics”, *Polymers*, vol. 14, no. 4, pp. 1-16, 2022.

[38] R. H. Myers, D. C. Montgomery, and C. M. Anderson-Cook, Response surface methodology: Process and product optimization using designed experiments, 4th Edition, John Wiley & Sons, 2016.

[39] M. M. Hasan, M. G. Rasul, M. I. Jahirul, and M. M. K. Khan, “Fast pyrolysis of macadamia nutshell in an auger reactor: Process optimization using response surface methodology (RSM) and oil characterization”, *Fuel*, vol. 333, no. 2, pp. 126490, 2023.

[40] G. Arun Prasad, P. C. Murugan W. Beno Wincy, and S. Joseph Sekhar, “Response surface methodology to predict the performance and emission characteristics of gas-diesel engine working on producer gases of non-uniform calorific values”, *Energy*, vol. 234, pp. 1-14, 2021.

[41] F. Jaliliantabar, B. Ghobadian, G. Najafi, R. Mamat, and A. Paolo Carlucci, “Multi-objective NSGA-II optimization of a compression ignition engine parameters using biodiesel fuel and exhaust gas recirculation,” *Energy*, vol. 187, pp. 1-15, 2019.

[42] Kocakulak, T., et al., "Predictive modelling and optimization of performance and emissions of an auto-ignited heavy naphtha/n-heptane fueled HCCI engine using RSM," *Fuel*, vol. 333, p. 126519, 2023.